Dissecting and modeling photic and melanopsin effects to predict sleep disturbances induced by irregular light exposure in mice

Jeffrey Hubbard[a,b], Mio Kobayashi Frisk[a,b], Elisabeth Ruppert[a,b], Jessica W. Tsai[c], Fanny Fuchs[a,b], Ludivine Robin-Choteau[a,d], Jana Husse[e], Laurent Calvel[a,b], Gregor Eichele[e], Paul Franken[f], and Patrice Bourgin[a,b,1]

[a]CNRS-Unité Propre de Recherche (UPR) 3212, Institute of Cellular and Integrative Neurosciences, 67084 Strasbourg, France; [b]International Research Center for ChronoSomnology, Translational Medicine Federation Strasbourg, Sleep Disorders Center, Strasbourg University Hospital, University of Strasbourg, 67000 Strasbourg, France; [c]Department of Biology, Stanford University, Stanford, CA 94305; [d]European Center for Diabetes Studies, 67200 Strasbourg, France; [e]Department of Genes and Behavior, Max Planck Institute for Biophysical Chemistry, 37077 Goettingen, Germany; and [f]Center for Integrative Genomics, University of Lausanne, 1015 Lausanne, Switzerland

Edited by Emmanuel Jean-Marie Mignot, Stanford University School of Medicine, Palo Alto, CA, and approved April 13, 2021 (received for review September 23, 2020)

Artificial lighting, day-length changes, shift work, and transmeridian travel all lead to sleep–wake disturbances. The nychthemeral sleep–wake cycle (SWc) is known to be controlled by output from the central circadian clock in the suprachiasmatic nuclei (SCN), which is entrained to the light–dark cycle. Additionally, via intrinsically photosensitive retinal ganglion cells containing the photopigment melanopsin (Opn4), short-term light–dark alternations exert direct and acute influences on sleep and waking. However, the extent to which longer exposures typically experienced across the 24-h day exert such an effect has never been clarified or quantified, as disentangling sustained direct light effects (SDLE) from circadian effects is difficult. Recording sleep in mice lacking a circadian pacemaker, either through transgenesis (*Syt10*$^{cre/cre}$*Bmal1*$^{fl/-}$) or SCN lesioning and/or melanopsin-based phototransduction (*Opn4*$^{-/-}$), we uncovered, contrary to prevailing assumptions, that the contribution of SDLE is as important as circadian-driven input in determining SWc amplitude. Specifically, SDLE were primarily mediated (>80%) through melanopsin, of which half were then relayed through the SCN, revealing an ancillary purpose for this structure, independent of its clock function in organizing SWc. Based on these findings, we designed a model to estimate the effect of atypical light–dark cycles on SWc. This model predicted SWc amplitude in mice exposed to simulated transequatorial or transmeridian paradigms. Taken together, we demonstrate this SDLE is a crucial mechanism influencing behavior on par with the circadian system. In a broader context, these findings mandate considering SDLE, in addition to circadian drive, for coping with health consequences of atypical light exposure in our society.

circadian and noncircadian | sleep–wake cycle | phototransduction | melanopsin | photoperiods

The nearly ubiquitous expression of circadian rhythmicity across species suggests that synchronizing physiology and behavior to Earth's light–dark (LD) cycle is critical for survival and essential for optimal functioning and health. With increasing environmental light pollution and the introduction of new technologies such as light-emitting diodes and connected devices, human photic behavior is increasingly uncoupled from the natural LD cycle. The resulting perturbations in sleep–wake architecture have led to the increased prevalence of circadian disorders, insomnia, daytime somnolence, mood alteration, and poorer cognitive performance (1–5), stressing the need for a greater and more mechanistic understanding of the photic regulation of sleep and behavior.

Light entrains the circadian pacemaker located in the suprachiasmatic nuclei (SCN), whose output signal generates an endogenous circadian sleep–wake rhythm aligned to the environmental LD cycle (6). However, light also exerts direct acute effects on sleep and waking, independent of the circadian system (7, 8). In nocturnal animals, such as most laboratory rodents, darkness administered for short periods (e.g., 1 h) acutely induces waking behavior, while the same length of light exposure promotes sleep (7). In circadian biology, these light- and/or dark-dependent changes were referred to as "masking," as they can conceal the sleep–wake rhythm generated by the clock output signal. Therefore, this direct and noncircadian photic regulation was primarily considered through its indirect consequences on circadian function rather than a process actively imposing itself on the expression of sleep and waking in a direct and important manner (9). This highlights the need for a better understanding of the significance of the direct photic regulation of sleep and waking in comparison to clock-driven influence.

The nonvisual effects of light are known to be mediated through different photoreceptive systems and neuronal pathways. Previous research led to the discovery of a novel retinal photoreceptor, melanopsin (Opn4), which is crucial for irradiance detection, maximally sensitive to blue light (480 nm), and expressed in a subset of intrinsically photosensitive retinal ganglion cells (ipRGCs) that convey nonimage-forming light information to the brain (10–12). These melanopsin ipRGCs project to various brain targets, which

Significance

Light pervasively affects physiology and behavior, especially the sleep–wake cycle (SWc), which is generated by clock signaling in the suprachiasmatic nuclei (SCN). Light synchronizes this clock and additionally exerts direct (circadian-independent) acute effects on sleep. However, it has never been clarified whether longer photic exposure, as experienced daily, might exert long-term sustained direct light effects (SDLE). Recording sleep in mice lacking a functional clock and/or the retinal photopigment melanopsin, we uncovered that circadian-driven input and SDLE equally contribute to SWc. SDLE were primarily mediated through melanopsin, with half relayed through SCN, redefining the latter's role. Modeling allowed SWc prediction under simulated jet lags, further demonstrating SDLE as an important mechanism to consider when managing health consequences of light exposure.

Author contributions: J. Hubbard, P.F., and P.B. designed research; J. Hubbard, M.K.F., E.R., J.W.T., F.F., L.R.-C., J. Husse, and L.C. performed research; J. Hubbard, M.K.F., E.R., and P.B. analyzed data; and J. Hubbard, M.K.F., G.E., P.F., and P.B. wrote the paper.

The authors declare no competing interest.

This article is a PNAS Direct Submission.

[1]To whom correspondence may be addressed. Email: pbourgin@unistra.fr.

This article contains supporting information online at https://www.pnas.org/lookup/suppl/doi:10.1073/pnas.2017364118/-/DCSupplemental.

Published June 21, 2021.

are thought to mediate light influence on physiology and behavior (13–15). Clock synchronization and circadian rhythm entrainment is mediated by projections to the SCN (16–18), whereas innervation of the sleep-promoting neurons of the ventrolateral preoptic area (VLPO) (19, 20) or the subparaventricular zone are thought to mediate light's direct effects on sleep, yet it remains to be clarified whether the SCN might also participate in mediating those direct photic effects. Moreover, the loss of melanopsin does not abolish these responses, demonstrating that other photoreceptors involved in vision, the rods and cones, also play a role (12). Furthermore, the loss of ipRGCs results in dramatic loss of nonvisual effects, indicating that these cells receive inputs from rods and cones and are also the principal conduit for nonvisual light input from these photoreceptors (12, 18, 21–23). However, the degree of overlap between these two systems for regulating nonvisual responses is not yet certain.

In recent years, the development of transgenic mouse models targeting these phototransduction pathways has revealed the pronounced effects of light and dark pulses of short duration on sleep and waking (11, 12, 24). Moreover, we previously showed that this acute and direct photic influence can be observed at all times of day (12). These observations raise the question as to whether longer periods of light and dark exposure, such as those of the 24-h LD cycle, exert sustained direct noncircadian effects, that is, continuous acute effects that could be observed over longer periods of time. One could postulate that the complete absence of light (constant darkness [DD] experiments) would allow for the extrapolation of the influence of sustained direct photic effects; however, this would not consider the possibility that the absence of light would lead to circadian disruption. Thus, under standard LD cycles, the contribution of direct noncircadian photic regulation in shaping the sleep–wake cycle has to date never been properly quantified due to the difficulty in disentangling it from the circadian effects.

In the current study, we sought to address three related issues: 1) the quantification of the respective contribution of circadian effects (CE) and sustained direct light effects (SDLE) in shaping the 24-h sleep–wake cycle; 2) the identification of the pathways underlying those effects (i.e., the respective role of the photoreceptive systems), melanopsin versus rods and cones, and the respective role of the SCN versus non-SCN brain relays as conduits for this direct photic regulation of the sleep–wake cycle; and 3) whether quantifying the respective contributions of CE and SDLE allows for the prediction of the nychthemeral sleep–wake distribution under unnatural LD cycles, such as those experienced during jet lag. Recording sleep in mice lacking a functional central clock either through SCN lesioning or *Bmal1* tissue-specific clock gene deletion and/or melanopsin-based phototransduction, we uncovered that CE and SDLE contribute in equal proportion to shaping the nychthemeral cycle. Furthermore, analyzing sleep in melanopsin-deficient mice with or without disabled SCN revealed that SDLE are primarily (>80%) mediated through melanopsin-based phototransduction, half of which passes via the SCN, implying a noncircadian function for the brain structure comprising the master circadian clock. To further validate our findings, these data were integrated into a model that accurately predicted 24-h sleep–wake distribution in mice exposed to a simulated "jet lag" or transequatorial travel paradigm.

Results

Nychthemeral Sleep–Wake Cycle Amplitude Is Decreased by Half in the Absence of Light or when Light Is Equally Distributed Across 24 h. To estimate overall light influence on the 24-h sleep–wake cycle amplitude, we recorded sleep electrocorticograms (ECoG) in animals in the absence of light or when light is equally distributed across 24 h. Here, and below, we defined the nychthemeral sleep–wake cycle (SWc) amplitude as the difference in non-rapid eye movement sleep (NREMS) amounts between 12-h light (day) and 12-h dark (night) periods. Similar analyses were performed using waking or rapid eye movement sleep (REMS) for calculating SWc amplitude, leading to comparable observations. Of note, hourly NREMS amounts across the 24-h period follow a more square-like distribution, therefore taking the 12-h LD difference is appropriate as an amplitude estimate. Furthermore, under constant darkness, the term "subjective light" defines the ZT0-12 period corresponding to the 12-h light phase of the preceding days, and the term "subjective dark" corresponds to the ZT12-24 period, that is, the 12-h dark phase of the preceding days, given that a circadian phase shift would be negligible during a single day of DD. Under DD, we found that SWc amplitude was reduced by ~1 h (Fig. 1 *B* and *C* and *SI Appendix*, Fig. S1*C*), representing 45% when compared with LD12:12, indicating that the 55% remaining was generated by the circadian drive. Another way to estimate the overall effects of light is to record sleep and waking under ultradian light/dark cycles, in which light and dark pulses are evenly distributed throughout the nychthemeron with pulse-induced effects on sleep superimposing on the circadian modulation. Thus, mice were exposed to consecutive 1-h light and 1-h dark pulses (LD1:1), which we previously used to analyze the acute direct effects of light according to the time of day (12). Next, a group of animals was exposed to consecutive pulses consisting of 3.5 h light and 3.5 h dark (LD3.5:3.5), an alternative condition in which L/D pulses are not aligned to 24 h (24, 25). Under LD1:1, LD3.5:3.5, and DD, NREMS amounts were noticeably different (*SI Appendix*, Fig. S1 *A–C*). With these two ultradian LD cycles, we assumed that the direct effects of alternating light and dark pulses nullified one another over time and that the residual SWc amplitude represented the remaining circadian influence. Remarkably, the circadian contribution under these two ultradian LD regimes were found to be within the same range as was calculated previously under LD12:12 (LD1:1, 50 ± 11% and LD3.5:3.5, 52 ± 7% versus 55% ± 6% in DD; *SI Appendix*, Fig. S1*D*). Thus, this decrease by half of the SWc amplitude demonstrates a crucial role for the direct influence of light in driving the nychthemeral sleep–wake distribution and further suggests that it can be sustained for longer periods of time, with acute and sustained DLE having very similar effects. However, under those conditions, it cannot be ruled out that the circadian system is not altered in the absence of light or under alternating light signals. Therefore, this underlines that the reduction of SWc amplitude observed here may also result from an alteration of CE, a question that our step-by-step approach below addresses.

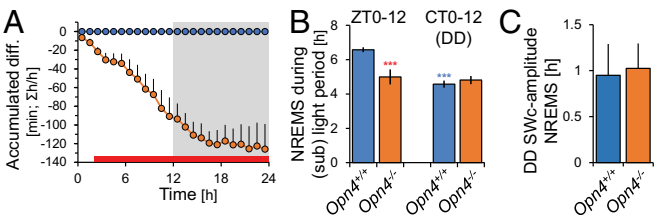

Fig. 1. Melanopsin-based SDLE contributes to approximately one-third of the SWc amplitude. (*A*) Dynamics of the accumulated differences demonstrate that *Opn4*$^{-/-}$ mice lose 2 h of NREMS per day, with a maximum effect (1.5 h) during the light period (average of 2 consecutive days under LD12:12). (*B*) NREMS amount during light period under LD12:12 (*Left*) is decreased in *Opn4*$^{-/-}$ and similar to that during subjective light period under DD in both genotypes (*Right*). (*C*) SWc amplitude in *Opn4*$^{+/+}$ and *Opn4*$^{-/-}$ mice under DD did not differ. These observations demonstrate that sleep loss during the light period and subsequent SWc amplitude decreases in *Opn4*$^{-/-}$ mice result from a lack of Opn4-based SDLE and not from a reduction in circadian signal. DD: sham *Opn4*$^{+/+}$ $n = 5$; sham *Opn4*$^{-/-}$ $n = 7$. Asterisks denote significant post hoc differences after ANOVA between LD conditions (blue) and the genotype (red).

SDLE Are Primarily Mediated by Melanopsin-Based Photoreception. Melanopsin has been shown to be the primary mediator of the acute direct influence of light on sleep and waking, with rods and cones playing only a minor role (for review, see ref. 7). To determine whether melanopsin-based direct photic influence would be sustained for longer periods, therefore contributing to the SWc, we assessed sleep in melanopsin-deficient mice ($Opn4^{-/-}$). Under LD12:12, mice lacking melanopsin, in comparison with wild-type (WT) animals, displayed a 1.5-h reduction in NREMS, similar to what we previously observed in these mice (12). This NREMS decrease constantly accumulated across the entirety of the 12-h light phase (Fig. 1*A*). The reduction in NREMS also continued during the dark period but to a lesser extent (0.5 h), thereby reducing SWc amplitude and resulting in a 37% decrease compared with WT controls ($Opn4^{+/+}$). In the context of SDLE, we interpreted this as a lack of melanopsin-driven input, assuming that CE were not impacted in these mice by a life-long loss of Opn4. We verified this latter point by confirming SWc amplitude under DD did not differ between mice either expressing melanopsin or not (Fig. 1*B*). Moreover, the accumulated NREMS loss during the 12-h light phase in $Opn4^{-/-}$ mice (Fig. 1*A*) was similar to the NREMS reduction observed during the subjective light period (CT0-12) under DD in both WT and $Opn4^{-/-}$ mice (Fig. 1*C*). Therefore, NREMS reduction in these animals resulted not from a circadian defect but a lack of direct photic influence, identifying that one-third (37%) of SWc amplitude was driven by Opn4-mediated SDLE.

One-Quarter of the Nychthemeral SWc Is Determined by SCN-Independent Sustained Direct Light Effects. The most straightforward method to eliminate the influence of CE on the sleep–wake distribution is to disable the central circadian pacemaker (SCN). To calculate the proportion of the SWc amplitude generated by SCN-signaling, we studied two groups of mice in which this structure had been either physically removed through thermolytic lesioning (SCNx) or rendered inert through the deletion of the clock gene *Bmal1* in the SCN ($Syt10^{Cre/Cre}Bmal1^{fl/-}$), which halts clock function while leaving the SCN physically intact (26). First, we performed a set of experiments to assess SCN functionality and to control for the putative limitations of each model; that is, lesion-induced structural damages as well as potential consequences of deleting *Bmal1* in Syn10-expressing cells outside the SCN.

Under DD conditions, SCNx mice were arrhythmic, which was confirmed by sleep ECoG recordings (Fig. 2*B*). We then verified that lesioning the SCN preserved the underlying phototransductive system, as the retinohypothalamic tract is in close proximity to the SCN. We ensured that underlying pathways were mostly preserved by SCN lesioning through injection of an anterograde tracer (cholera toxin subunit-B [CtB]) into the posterior chamber of the eye. Even if it was not possible to conclude that the lesions fully spared all retinal projections, we found that they were conserved to a similar extent as for sham-lesioned controls, both in cases of highly innervated brain structures such as the ventral geniculate leaflet nucleus and the superior colliculus as well as areas less innervated but critically relevant for sleep regulation such as the VLPO (*SI Appendix*, Fig. S2 *A–D*). The efficacy of SCN lesioning was confirmed postmortem with arginine vasopressin (AVP) and DAPI whole-brain staining (*SI Appendix*, Fig. S2 *E–H*).

Our second mouse model, $Syt10^{Cre/Cre}Bmal1^{fl/-}$, had been previously shown to be arrhythmic in both SCN clock gene expression and general locomotor activity under DD (26). In the present work, we further confirmed the effective abolishment of the SCN clock in these mice through actimetry and ECoG recordings under constant darkness, which revealed a total loss of sleep–wake rhythmic activity as well as abolishing NREMS differences between subjective light and dark periods (Fig. 2*B*). Then, to assess the extent to which SCN neurons remained responsive to light, we quantified c-Fos expression, a marker of neuronal activation, in response to a 1-h light pulse administered during the dark period (Zeitgeber time [ZT] 15 to 16). This is a time of day when light-induced c-Fos immunoreactivity and the resulting phase delay of the circadian rhythms of locomotor activity are known to be maximal (11, 12). Overall, the light pulse–induced c-Fos immunoreactivity was dramatically decreased in $Syt10^{Cre/Cre}Bmal1^{fl/-}$ as compared with both control groups ($Syt10^{Cre/Cre}Bmal1^{+/-}$ and WT mice; Fig. 2*A*). It should be noted that a few SCN cells in the retinorecipient part of the SCN were still reactive to light in $Syt10^{Cre/Cre}Bmal1^{fl/-}$, but no remaining c-FOS expression was observed in the shell part of the SCN, which receives input from the core and corresponds to the clock output region (27), suggesting a lack of noncircadian phototransduction through this structure. This disabling of the system was supported by the observation in these mice of a lack of AVP immunoreactivity, a neuropeptide present in SCN cells regulating interneuronal coupling and circadian behavior (28, 29), while AVP immunoreactivity could still be detected in surrounding structures (Fig. 2 *A*, *iii* and *v*). Thus, taken together, these results confirm the lack of functionality of the SCN and the complementarity of these two approaches (lesioning versus conditional clock gene deletion) to control for the putative limitations inherent to each one, demonstrating their pertinence to study SDLE in the absence of circadian influence.

Under LD12:12 conditions, SCN-disabled mice revealed clear differences in the 24-h time course of NREMS (Fig. 2*C*). Overall, NREMS amounts were still higher during the light period, although they were significantly reduced as compared with controls. Taking differences in the SWc amplitude between both sham and SCNx animals, we were able to determine the percentage of photic information passing through the SCN. The difference in SWc amplitude between controls (WT and $Syt10^{Cre/Cre}Bmal1^{+/-}$ mice) and $Syt10^{Cre/Cre}Bmal1^{fl/-}$ was identical, further validating the estimation of the contribution of the SCN. SWc amplitude under LD12:12 was ∼2.5 h in all control groups (WT and $Syt10^{Cre/Cre}Bmal1^{+/-}$). In comparison with controls, the disablement of the SCN induced a profound reduction in SWc amplitude that was remarkably similar in both models, 76.4 and 76.8% in SCNx and $Syn10^{Cre/Cre}Bmal1^{fl/-}$, respectively (Fig. 2*D*). Of note, about one-quarter of the SWc amplitude was conserved in these two models. This indicates that light exerts a sustained direct noncircadian effect, strong enough to uphold a 24-h organization of sleep and waking in the absence of SCN-generated circadian rhythms and that SCN-driven signaling is responsible for three-quarters of the SWc amplitude observed under LD12:12.

The SCN Acts Not Only as a Clock but Mediates Half of the Sustained Direct Alerting Effects. Thus far, we demonstrated that 77% of the SWc amplitude depends on SCN output, and we could therefore assume this to be the result of its inherent clock function. However, we could not rule out that part of this SCN-dependent SWc amplitude arose from direct effects of light mediated through the SCN independently of clock mechanisms. To separate melanopsin-based SDLE mediated through the SCN from pathways external to these nuclei, we examined SWc amplitude in animals lacking melanopsin photopigment ($Opn4^{-/-}$) with or without a functional SCN (SCNx), which demonstrated that Opn4-based phototransduction accounted for 18% of the SWc amplitude through pathways outside of the SCN and 19% within (Fig. 3 *A* and *B*). Thus, our observations confirmed that nearly half (49%) of SDLE were mediated through SCN pathways, identifying that this structure, beyond its clock function, significantly influenced vigilance states (Fig. 3*C*).

Interestingly, the flattened SWc amplitude observed in SCN-ablated mice resulted mainly from a decrease in waking during the dark phase. Indeed, in nocturnal animals such as mice, darkness is known to exert a wake-promoting effect, whereas in humans, light has been shown to acutely promote alertness, with the highest efficiency of blue light centered around 480 nm, within the spectral response peak of melanopsin (4, 30). Therefore, we calculated

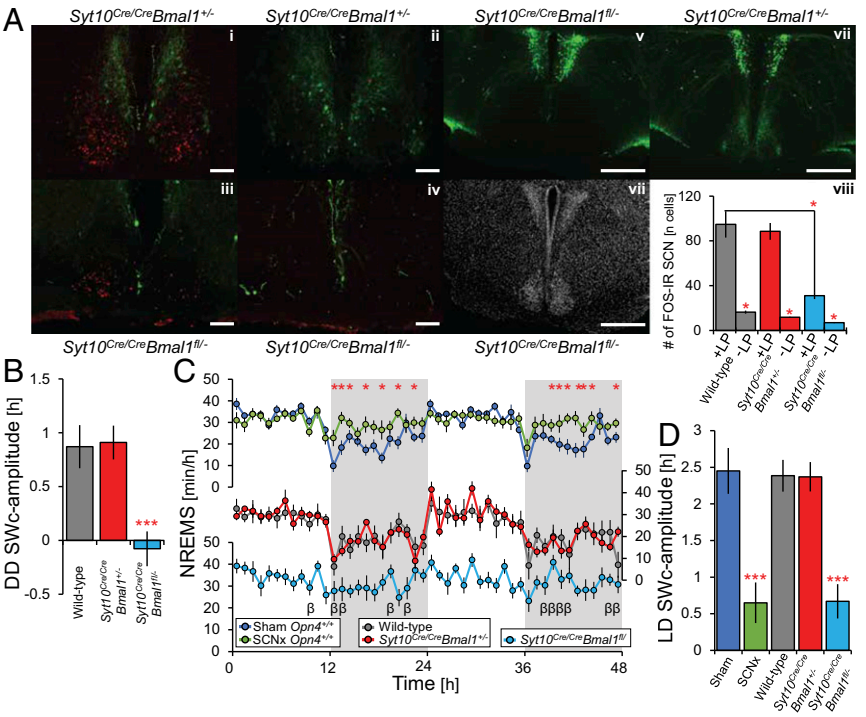

Fig. 2. SCN-independent direct effects of light determine about one-quarter of SWc amplitude. (*A*) Effects of the L pulse administered during the habitual dark period (ZT 15 to 16) on c-Fos immunoreactivity in the SCN of the different mice genotypes. c-Fos immunoreactive cells are labeled in red and AVP immunoreactive cells in green. Light pulse– (+LP; at ZT 15 to 16) induced c-FOS immunoreactivity (red) in the SCN in (*i*) *Syt10*$^{Cre/Cre}$*Bmal1*$^{+/-}$ controls. Light-induced c-Fos immunoreactivity was partially conserved in the retino-recipient (core) but absent in the clock output region (shell) in (*iii*) *Syt10*$^{Cre/Cre}$*Bmal1*$^{fl/-}$ demonstrating the alteration of SCN response to photic information. No c-FOS induction was seen in the absence of a light pulse in both *Syt10*$^{Cre/Cre}$*Bmal1*$^{+/-}$ controls (–LP; *ii*) and *Syt10*$^{Cre/Cre}$*Bmal1*$^{fl/-}$ (–LP; *iv*). Moreover, in *Syt10*$^{Cre/Cre}$*Bmal1*$^{fl/-}$, AVP expression (a marker of clock output in the shell part of the SCN, green) is abolished in the SCN (*v*) (that remains structurally intact; *vi*: DAPI staining, gray) but not in surrounding areas (*iii–v*). AVP expression in the SCN is preserved in *Syt10*$^{Cre/Cre}$*Bmal1*$^{+/-}$ (*i*, *ii*, and *vii*). (Scale bars, 100 μm in *A*, *i–iv*, 500 μm in *A*, *v–vii*.) (*Bottom Right*) Histogram represents quantification of light-induced c-FOS expression in SCN neurons (*viii*). The light pulse–induced c-Fos in the SCN in similar proportion in all control groups (*Syt10*$^{Cre/Cre}$*Bmal1*$^{+/-}$, WT). WT $n = 6$; *Syt10*$^{Cre/Cre}$*Bmal1*$^{+/-}$ $n = 8$; and *Syt10*$^{Cre/Cre}$*Bmal1*$^{fl/-}$ $n = 6$. Data are expressed as mean ± SEM. Two-way ANOVA: $P_{light\ pulse} \leq 0.001$; $P_{genotype} \leq 0.001$, post hoc *t* test: $^*P < 0.05$). Raw multichannel images are available (see ref. 40). (*B*) Difference in NREMS amounts between subjective light and dark periods (SW amplitude) under DD conditions in *Syt10*$^{Cre/Cre}$*Bmal1*$^{fl/-}$ mice and their controls. SW amplitude of SCN-disabled mice (*Syt10*$^{Cre/Cre}$*Bmal1*$^{fl/-}$) did not significantly differ from zero confirming SW arrhythmicity in these mice. Values represent means ± SEM. (*C*) Time course of NREMS in SCNx, *Syt10*$^{Cre/Cre}$*Bmal1*$^{fl/-}$, and their controls for 2 d under LD12:12. (*D*) SWc amplitude under LD in SCN-invalidated mice and their controls (amplitude defined as the difference in NREMS amounts between light [day] and dark [night] periods, average of 2 consecutive d under LD12:12). The lack of a functional SCN/clock affects the SWc by reducing its amplitude by 1.8 h in SCNx mice (LD NREMS difference: 39 ± 13 min) and by 1.7 h in SCN-disabled mutants (LD NREMS difference: 40 ± 16 min). Immunohistochemistry experiments: $n = 3$ to 4 per group/condition. ECoG experiments: sham *Opn4*$^{+/+}$ $n = 9$; SCNx *Opn4*$^{+/+}$ $n = 10$; WT $n = 7$; Syt10$^{Cre/Cre}$*Bmal1*$^{+/-}$ $n = 7$; and Syt10$^{Cre/Cre}$*Bmal1*$^{fl/-}$ $n = 10$. Psi symbols denote *Opn4* genotype post hoc differences, delta denote SCN condition post hoc difference, and beta denote *Bmal1* versus control post hoc difference.

the power spectral density of the ECoG to quantify theta (7 to 10 Hz) and gamma (40 to 70 Hz) activities, known to be correlates of exploratory behavior and alertness (31–33). Remarkably, both were significantly decreased in each of the SCN-deficient models, specifically during the 12-h dark period of LD12:12 (*SI Appendix*, Fig. S3), indicating that the alerting effect of darkness in nocturnal animals (inverted in diurnal species) is primarily signaled though the SCN.

SDLE and CE Equally Contribute to Shaping the 24-h SWc. Although we have shown that SDLE were primarily mediated by Opn4-dependent pathways, a possible contribution of rods- and cones-based photoreception could not be excluded. To address this, we calculated SWc amplitude in SCNx *Opn4*$^{-/-}$ mice, giving us an estimate of rod/cone-based SDLE mediated outside the SCN, which was found to be low (~5%; Fig. 3*B*). However, these values were not significantly different from zero (one-sample signed rank test, $P = 0.22$), signifying that their contribution is likely negligible. Summarizing these findings indicated that 42% of the SWc amplitude was determined by SDLE, that is, the SDLE contribution we previously calculated in the absence of light under DD in WT animals (45%), and we therefore attributed this 3% difference to a possible contribution of SCN-dependent rod/cone-based phototransduction (Fig. 3*C*). This confirms the results from our initial DD experiment on the role of light in determining the SWc and further demonstrates that optimal functioning of SDLE requires both melanopsin-based phototransduction and a functional SCN in addition to other brain relays such as the VLPO.

These results encompass different photic and circadian regulatory factors (CE versus SDLE, Opn4 versus rods/cones, and SCN versus non-SCN–mediated transmission), leading us to conclude that SDLE and CE are nearly equal in influencing 24-h sleep–wake distribution. This estimate was corroborated by analysis of WT mice under the previously mentioned ultradian cycles in which light and dark pulses were evenly distributed over the nychthemeral cycle, indicating approximate SWc amplitude values of 50 and 48% for LD1:1 and LD3.5:3.5, respectively (*SI Appendix*, Fig. S1). Finally, regarding other vigilance states, the contributions of CE and SDLE to REMS distribution were similar to those we calculated for NREMS (*SI Appendix*, Fig. S4). Overall, the remarkable coherence of our results across experimental conditions strengthens the robustness of our observations on an equal

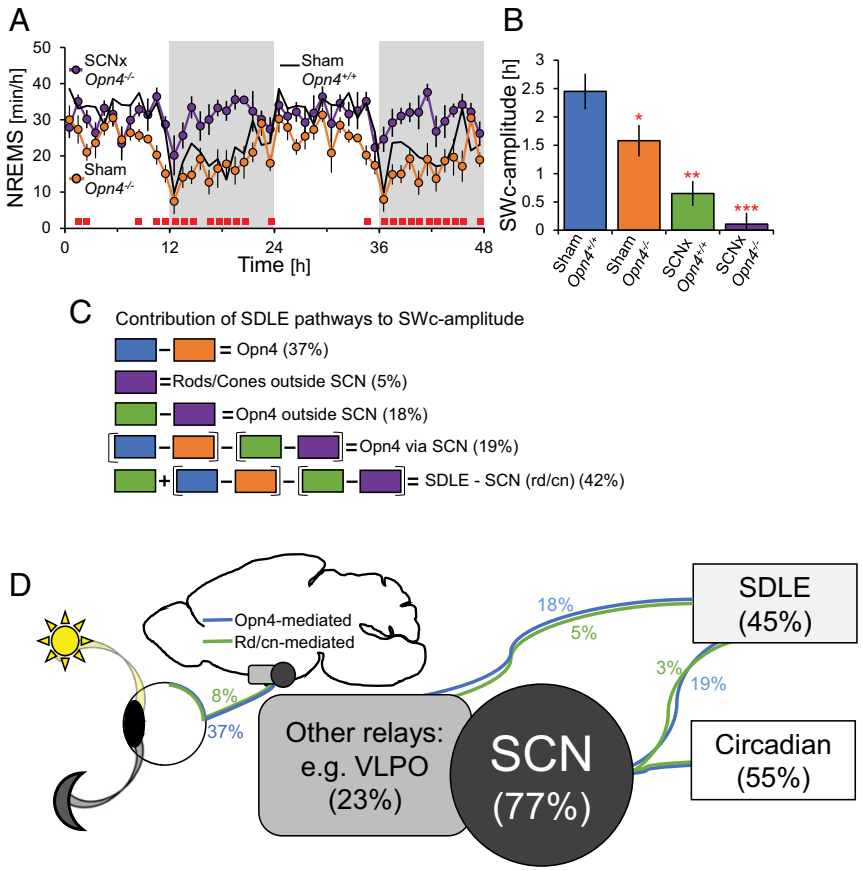

Fig. 3. The SCN, beyond its clock function, mediates part of the sustained direct effects of light. (*A*) Time course of NREMS during LD12:12 showed sham and SCNx *Opn4*$^{-/-}$ mice were significantly different (two-way repeated measures ANOVA, $_{\text{group x time}}$; $P < 0.001$) as the time course of NREMS over 24 hr is flattened. (*B*) SWc amplitude between sham and SCNx mice with or without melanopsin. SCNx *Opn4*$^{-/-}$ do not significantly differ from zero. (*C*) Intergroup differences in SWc amplitude to calculate percentage contributions to SWc amplitude of the different pathways involved. (*D*) Respective contribution (%) of the different pathways involved in shaping the SWc: contribution of CE versus SDLE (boxes), SCN versus other brain relays, and SDLE contribution mediated by melanopsin- (blue) versus rod/cones-based (green) photoreception (*Materials and Methods*). The red squares (line) in *A* represent significant post hoc differences between groups. Asterisks represent paired *t* test significance from sham WT mice. LD12:12: sham *Opn4*$^{+/+}$ $n = 9$; sham *Opn4*$^{-/-}$ $n = 7$; SCNx *Opn4*$^{+/+}$ $n = 10$; and SCNx *Opn4*$^{-/-}$ $n = 8$.

contribution of CE and SDLE as well as on the respective role of the different underlying pathways.

We summarized our findings in a model presented in Fig. 3 *C* and *D*, integrating the respective contributions of the main phototransduction pathways regulating the natural SWc through use of SWc amplitude as a proxy. Briefly, the role of each component was calculated based upon intergroup differences of this measure as the degree of SWc amplitude reduction is dependent on the phototransduction element being removed in each. The contribution of the SCN (combined SDLE and CE) was estimated through the SWc amplitude difference between SCN-disabled mice and controls. In addition, the contribution of melanopsin-dependent SDLE was calculated based on the SWc amplitude reduction observed in melanopsin-deficient mice (given that CE were conserved in these mice). The percentage mediated through the SCN was estimated in SCNx animals with the difference between those either possessing or lacking melanopsin. These two latter calculations allowed us to derive the proportion of Opn4-based SDLE mediated through the SCN. The removal of both melanopsin and SCN (SCNx *Opn4*$^{-/-}$) gave us the contribution of the rods/cones-dependent SDLE mediated through brain relays outside of the SCN (as it was the only pathway conserved), whereas the one mediated through the SCN was negligible. Finally, the calculations under DD, LD1:1, LD3.5:3.5, and from our intergroup comparisons under LD12:12 converged toward an estimation that SDLE and CE influence is nearly equal. (Fig. 3*D*). In summary, the model allowed us to describe the contribution of all dissected mechanisms: CE, SDLE, and underlying pathways of melanopsin- versus rod/cone-based photoreception, relayed through SCN versus non-SCN brain structures.

Modeling Predicts 24-h Sleep–Wake Distribution under Simulated Jet Lag. We then integrated CE and SDLE contributions (55 and 45%, respectively) into a model aimed at estimating whether these respective effects could estimate overall sleep–wake distribution under other light/dark paradigms. As this was the first time SWc amplitude had been used to derive such a model, we chose two light/dark schedules simulating either transequatorial (i.e., rapid seasonal change) or transmeridian (intercontinental) travel, conditions commonly experienced in modern society. In WT mice exposed to a shortened photoperiod (transequatorial; LD8:16), we found the overall model estimation and shape of the nychthemeral SWc to be similar to values obtained from ECoG recordings (Fig. 4 *A* and *B*).

Next, a separate group of mice were subjected to a simulated westward transmeridian travel with an 8-h prolongation of the dark period followed by a shifted LD12:12 cycle (Fig. 4 *C*, *Top*). Whereas in the first experiment we assumed the SCN output not to be affected, this condition included an additional factor, as shifting the LD cycle induces a phase adjustment of the clock to

the new LD cycle (i.e., jet lag). Indeed, sleep recordings under this condition showed that resynchronization to the new LD12:12 cycle took ~96 h (Fig. 4*C*). This same time delay was observed when evaluating locomotor activity patterns, which fully resynchronized by day 5 following the jet lag (for example, see *SI Appendix*, Fig. S5). Therefore, we assumed stable entrainment to the new LD cycle across 4 d with a linear shift over this period of time of ~1.10/12 h (derived from a best fit of the observed shift based on NREMS data). To calculate the estimated NREMS time course, hourly values were multiplied by CE (55%) and SDLE (45%) contributions (as in Fig. 3*D*) and plotted in 3-h bins (*Materials and Methods*). Remarkably, when integrating this constant (phase shift of CE) into the model, the predicted 24-h NREMS distribution (Fig. 4*C*, purple line) closely followed the observed changes in NREMS across the entirety of the experiment (11 d; Fig. 4*C*, red line), although an overall increasing trend in NREMS over the days following resynchronization could not be fully captured by the model. Furthermore, the model predicted the SWc amplitude dynamics, substantiated by linear regression of predicted versus observed values of these changes across subsequent days (Fig. 4*D*). Indeed, it identified with greatest accuracy the SWc amplitude dynamics, which were initially attenuated as a result from CE and SDLE being out of phase and partially negating one another at certain times of the day before resynchronization (see blue and green lines in Fig. 4 *C*, *Bottom*). Taken together, these results establish the robustness of this model, further validating our findings of an equal contribution of CE and SDLE in shaping nychthemeral sleep and wake distribution.

Discussion

In this study, we demonstrate, contrary to the prevailing assumption, that only half of the overall changes to SWc amplitude are generated by a circadian signal, with SDLE being an equally important mechanism. Indeed, these findings challenge our current understanding of how photic input influences the amplitude and pattern of the SWc. Furthermore, we show that SDLE is capable of compensating for the absence of clock-driven influence to help maintain sleep–wake distribution aligned with external LD cues.

This study was designed to investigate the sustained effects of light on sleep–wake distribution, but we acknowledge that other factors potentially influence the distribution of vigilance states. In the current study, we focus only on CE and SDLE, as the experiments were conducted under controlled laboratory conditions, which do not account for other environmental factors known to influence sleep and waking. Indeed, the homeostatic process, defined as an accumulation of sleep pressure with time spent awake and its release during sleep, is another key regulator (34). However, our results on SWc amplitude and the derived model were based on 12-h values of sleep/wake states, which likely contributes to its accuracy, with the kinetics of the homeostatic process being much faster than 12-h periods in mice (35), contrary to humans. Another limitation of this study is the lack of female animal inclusion. While it has been shown that young adult female mice display changes in overall sleep and waking behavior compared with males, circadian rhythms and 24-h sleep–wake distribution in animals of this age are unaffected (36). Furthermore, we acknowledge that these mice are recorded in socially isolated conditions, with identical luminance levels across the light period, and one should be aware that the relative contributions of CE and SDLE and resulting SWc amplitude could be influenced by behavior and social interaction such as mating, foraging, or other ecological conditions. Finally, the present quantification of these CE and SDLE contributions in shaping the SWc, and the resulting modeling, was designed based on controlled conditions to provide a unique framework intended to evolve with the integration of additional environmental factors (e.g., ambient temperature, noise, etc.), which may allow a more precise model to be designed and increase the prediction of sleep–wake distribution at smaller time scales, also facilitating its translation to humans and other species.

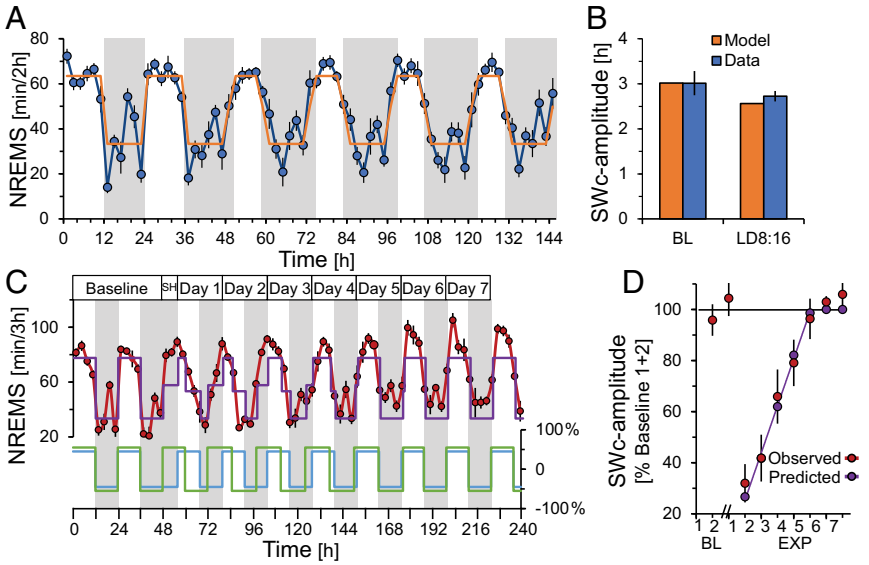

Fig. 4. Prediction of nychthemeral NREMS distribution under simulated transequatorial and transmeridian jet lag. (*A*) Time course of NREMS in WT mice under 48 h of LD12:12 followed by 4 d under LD8:16, simulating a transequatorial travel, with observed values (blue; min/2 h) and predicted values (orange; min/2 h). (*B*) SWc amplitude from prediction (orange) and from recorded animals (blue) under baseline (first 2 d under LD12:12) followed by 4 d under LD8:16. (*C*) Time course of NREMS in WT mice under 48 h of LD12:12 followed by 7 d under a simulated 8-h westward "jet lag". The predicted values of daily NREMS distribution (purple) based on the model integrating a shift of 1.1/12 h described in Fig. 3*D*, combining CE (blue) and SDLE (green), are shown. Daily NREMS distributions are obtained from sleep recordings (red) and are expressed as min/3 h. SH = shift (jet lag). (*D*) SWc amplitude under baseline (BL; LD12:12) and simulated 8-h westward and "jet lag" conditions across experimental (EXP) days. A linear regression of SWc amplitude is plotted to illustrate resynchronization to the new LD (R^2 = 0.99). The values in red obtained from recorded animals perfectly fit the predicted values in purple (one-way repeated measures ANOVA, $P_{group \times time}$ = 0.28). The dashed line represents the average baseline value at 100%. All values represent mean ± SEM, LD8:16: n = 7; jet lag: n = 9.

Our findings clearly redefine the role of the SCN, which should be seen not only as the orchestrator of circadian rhythms but a critical component of the direct photic regulation of alertness. Deciphering the molecular mechanisms behind circadian and direct photic processes within SCN cells will be crucial for our understanding of how environmental signals interplay with endogenous clock-driven mechanisms for optimal physiological and behavioral functioning. Furthermore, considering that numerous advancements in chronobiology have arisen from the interpretation that observed changes in animals with SCN lesions were solely attributed to the removal of the endogenous pacemaker, the present observations should encourage revisiting some of these conclusions (37). In addition, our findings emphasize the role of melanopsin-based phototransduction, as compared with rods and cones, in mediating the direct effect of light on sleep–wake behavior. This corroborates current literature on the photic regulation of behavior and identifies melanopsin phototransduction signaling as a potentially new pharmacological target for the manipulation of sleep and alertness (7).

This straightforward model emphasizes that optimal functioning requires CE and SDLE to be in phase with one another. Although these data and the proposed model are derived from experiments performed in nocturnal laboratory mice, the conservation of the circadian system and melanopsin-based phototransduction across mice and humans allow us to provide a conceptual framework for future studies in basic and clinical research. However, one should be aware that the interpretation of an equal contribution of CE and SDLE to shaping the 24-h SWc might differ in humans, as the weight of each of these two factors might be different in humans. Indeed, the present findings provide an explanation for the physiological and behavioral disturbances induced by the exposure to inappropriate lighting commonly observed in today's society, currently ascribed solely to a misalignment of the behavior relative to circadian time (1, 2). This could be used as a basis to optimize societal lighting and minimize light pollution as well as its application in certain medical conditions. Indeed, current therapeutics for circadian rhythm sleep disorders (CRSD) are based upon enhancing circadian reentrainment of the clock (5, 38). Our present findings, however, suggest taking into account the direct noncircadian effects of light as a key factor of CRSD management, as the insufficient consideration for SDLE possibly participates in the high rate of unsuccessful treatment (38). Finally, these observations could be an invaluable resource for improving other sleep disturbances, especially in facilitating adaptation to travel across time zones or to extreme latitudes, shiftwork, continuous screen exposure using modern media, or other concomitants of life in modern society.

Materials and Methods

Animals. All experiments were performed on young adult male mice using 1) *Opn4*$^{-/-}$ and WT littermate controls (12) on a C57BL/6 × 129Sv genetic background and 2) *Syt10*$^{Cre/Cre}$*Bmal1*$^{fl/-}$ on a C57BL/6 background (26), animals rendered arrhythmic through a conditional deletion of the clock gene *Bmal1* in the SCN using a Syt10 Cre driver (26) (from the Max Planck Institute for Biophysical Chemistry). Briefly, Syt10^{Cre} mice were crossed to a mouse line carrying a conditional allele of Bmal1, allowing Cre-mediated deletion of the exon encoding the BMAL1 basic helix–loop–helix domain (*Bmal1*$^{fl/fl}$). To generate experimental animals (*Syt10*$^{Cre/Cre}$*Bmal1*$^{fl/-}$), *Syt10*$^{Cre/Cre}$*Bmal1*$^{fl/+}$ females were crossed to *Syt10*$^{Cre/Cre}$*Bmal1*$^{fl/-}$ males. As controls, littermates of the genotype *Syt10*$^{Cre/Cre}$*Bmal1*$^{+/-}$ were used. To control for both the Cre driver and the heterozygosity of *Bmal1*, we verified that *Syt10*$^{Cre/Cre}$*Bmal1*$^{+/-}$ and WT mice displayed similar locomotor activity, ECoG, and sleep–wake patterns. All procedures complied with the local and international rules for the Care and Use of Laboratory Animals and were approved by the ethical committees for animal research (protocol no. B6748225 registered at the French Research Ministry). The animals were maintained under environmentally stable conditions (LD12:12; 25 ± 0.5 °C, food and water ad libitum). The genotype was validated by PCR: *Opn4*$^{+/+}$ and *Opn4*$^{-/-}$; primers: Mel4: 5′–TCA TCA ACC TCG CAG TCA GC–3′; Mel2: 5′–CAA AGA CAG CCC CGC AGA AG–3′; TodoNeo1: 5′–CCG CTT TTC TGG ATT CAT CGA C–3′ (from Sigma Life Science); *Syt10*$^{Cre/Cre}$*Bmal1*$^{fl/-}$ and *Syt10*$^{Cre/Cre}$*Bmal1*$^{+/-}$ and WT: *Bmal* flox forward: 5′-ACT GGA AGT AAC TTT ATC AAA CTG-3′; *Bmal* reverse: 5′-CTG ACC AAC TTG CTA ACA ATT A-3′; *Bmal* knockout forward: 5′-CTC CTA ACT TGG TTT TTG TCT GT-3′; *Syt10* forward: 5′-AGA CCT GGC AGC AGC GTC CGT TGG-3′; *Syt10* reverse: 5′-AAG ATA AGC TCC AGC CAG GAA GTC-3′; and *Syt10* KI forward: 5′-GGC GAG GCA GGC CAG ATC TCC TGT G-3′. The experimenters were blind to the experimental group and condition when analyzing the data such as sleep scoring or the quantification of c-Fos immunoreactivity.

Surgery.

Lesion of the SCN. The lesioning of the SCN was performed using a thermolytic probe, inserted at +3.6 mm; dorsoventral: +0.95 mm (39). Once lowered into the brain, heating was applied to the probe using a generator (Radionics Lesion Generator System) that allowed for precise control over voltage and temperature. Specifically, these lesions were achieved by heating the 250-μm tip of a TCZ electrode (Radionics) to 55 °C for a duration of 20 s. In order to control for the insertion of the probe into the brain tissue, the same surgery and procedure was completed in sham control mice (the electrode was lowered into the brain using the same stereotactic coordinates) but without using the lesion generator. SCNx and sham control mice were then implanted with ECoG and electromyography (EMG) electrodes (see below) for sleep recording.

ECoG implantation. Before undergoing implantation, mice were anesthetized with an intraperitoneal injection of ketamine 80 mg/kg and xylazine 7 mg/kg. Male *Opn4*$^{-/-}$ (n = 16), *Opn4*$^{+/+}$ (n = 19), *Syt10*$^{Cre/Cre}$*Bmal1*$^{fl/-}$ (n = 10), *Syt10*$^{Cre/Cre}$*Bmal1*$^{+/-}$ (n = 7), and *WT* (n = 7) mice were implanted with a classical set of electrodes (two ECoG, one reference, and two EMG) in order to record vigilance states using previously published methods (12). Mice were given a minimum of 14 d to recover from surgery and habituate to the sleep recording. The animals were recorded simultaneously using commercially available hardware and software (Micromed France, SystemPLUS Evolution version 1092; Compumedics PSG4, Compumedics).

Experimental Design. After surgery, different groups of mice were exposed to the following light/dark conditions: 1) LD12:12, 2) DD, 3) LD1:1, 4) LD3.5:3.5, 5) simulated transequatorial jet lag (LD8:16), and 6) simulated transmeridian jet lag (8-h prolongation of darkness followed by LD12:12). For anatomy experiments, mice were exposed to a either a 1-h light pulse from ZT 15 to 16 or darkness at the same time.

Sleep and Wake Analysis.

Locomotor activity monitoring. General activity was monitored using a standard infrared motion detector, and data were analyzed using the ClockLab software package (Actimetrics). SCNx and *Syt10*$^{Cre/Cre}$*Bmal1*$^{fl/-}$ mice were recorded for at least 10 d under LD12:12 followed by 2 wk under DD to measure their free running period to confirm the loss of circadian rhythmicity. *Syt10*$^{Cre/Cre}$*Bmal1*$^{+/-}$ mice were also recorded under the same conditions to confirm that they display a circadian pattern of locomotor activity similar to those of WT. The actimetry recordings were also performed (in parallel to ECoG recordings).

Sleep Scoring and Spectral Analysis of the ECoG. ECoG and EMG signals were acquired at 256 Hz and stored as continuous data streams. Vigilance states were scored into 4-s epochs using both ECoG and EMG signals based on standard criteria (32). The behavior in each of these 4-s epochs was classified as waking REMS or NREMS by visual inspection of the ECoG and EMG signals. The scoring was performed without information on the recording condition and genotype. The time spent in each of the vigilance states was averaged over 5 m and 1, 12, and 24 h in order to calculate intergroup differences. Spectral analysis was performed on raw signals every 4 s to which a Hamming window had been applied using a discrete Fourier transform. This produced power spectra between 0 and 128 Hz separated into 0.25 Hz bins. Dynamic changes in waking behavior were analyzed for theta (6 to 9 Hz) and gamma (40 to 70 Hz) frequencies and referenced to time periods where values were lowest (ZT 4 to 7).

Model Parameters for Disturbed Light Condition Experiments. The calculations for disturbed light conditions (Fig. 4) were based on the percentages determined under LD12:12 (Figs. 2 and 3) for mice lacking either a functional SCN or melanopsin. Briefly, under the light periods, the NREMS amounts are presumed to be due to photic influence of the circadian (55% CE) and noncircadian (45% SDLE), transduction systems. For baseline and experimental LD8:16 conditions, the following formula was used:

$$\text{Light period} = \left(\text{NREMS}_{\text{total}} * 0.55\right) + \left(\text{NREMS}_{\text{total}} * 0.45\right)$$

$$\text{Dark period} = \left(\text{NREMS}_{\text{total}} * 0.55\right).$$

For the jet lag experiment (Fig. 4 *C* and *D*), a CE shift of 1.1 h per 12 h was used. To achieve this, NREMS hourly values were split into 100 even bins (36 s). Subsequent days accounted for this change:

$$\text{Light period} = \sum\left[\left(\text{NREMS}_{\text{bin}} * 0.55\right) + \left(\text{NREMS}_{\text{bin}} * 0.45\right)\right]$$

$$\text{Dark period} = \sum\left[\text{NREMS}_{\text{bin}} * 0.55\right];$$

the values were then collapsed into hourly NREMS amounts. The model is denoted in purple in Fig. 4*C* and the CE and SDLE contributions in green and blue, respectively.

Anatomical Studies.

Immunostaining. After the completion of the protocol, mice were deeply anesthetized with CO_2 and perfused with 0.1 M phosphate-buffered saline (PBS) pH 7.4 followed by transcardial fixation for 15 min with 4% paraformaldehyde in PBS, pH 7.4. In order to study c-Fos immunoreactivity in response to light in *Syt10*$^{Cre/Cre}$*Bmal1*$^{fl/-}$ ($n = 3$), *Syt10*$^{Cre/Cre}$*Bmal1*$^{+/-}$ ($n = 4$), and WT ($n = 3$) animals, the euthanasia occurred at the conclusion of a 1-h light pulse administered at ZT 15 and without a light pulse as a negative control. SCNx and sham animals were euthanized 48 h after intraocular injection of CtB (see *Retinal Tract Tracing*). To control for SCN lesion size and the conservation of retino-cerebral projections, immunohistochemistry was used in SCNx and sham-lesioned animals to stain AVP, DAPI, and CtB. To evaluate SCN cells reactivity to light in *Syt10*$^{Cre/Cre}$*Bmal*$^{fl/-}$ and their controls, c-Fos expression was quantified in the SCN with AVP staining. The procedure was carried out as described previously (12). After dehydration in 30% sucrose for 48 h, the brains were frozen and cut in a freezing microtome. Free-floating slices, brought to room temperature, were rinsed three times (5 min each) in 0.1 M PBS (pH 7.0), incubated in 5% normal donkey serum (Normal Donkey Serum, 017–000-121 Jackson ImmunoResearch) and 0.25% Triton X-100 (TX) in PBS for 1 h, and then incubated overnight at 4 °C with primary antibodies (rabbit anti-c-Fos IgG, SC52 Santa Cruz Biotechnology, diluted 1:1,000; guinea pig anti-AVP, T-5018 Bachem, 1:2,000; and goat pAb anti-ctB, Calbiochem© 227040, 1:1,000) in a solution containing 0.25% TX in PBS. The following day, sections were rinsed three times (10 min each) in PBS before incubation with secondary antibodies (goat anti-rabbit IgG Alexa 555, Invitrogen 10373021, 1:500; donkey anti-guinea pig conjugated Cy5, Jackson ImmunoResearch, 706–175-148, 1:200; and donkey anti-goat conjugated Alexa 555, Invitrogen A21432, 1:500) in a solution containing 0.25% TX in PBS for 2 h. They were then rinsed three times (10 min each) in PBS and finally mounted on slides, allowed to air dry at room temperature, and cover slipped with mounting solution (glycerol 50%, 0.1 M PBS 50%, and DAPI 1:500, Sigma-Aldrich D9542). The omission of the primary antibody abolished all staining (control).

Photomicrographs and Quantification. Immunostainings were analyzed using a microscope equipped with appropriate filter settings for detecting Cy5, Alexa 555, and DAPI. Fluorescence images were obtained via a nonconfocal microscope (DMRXA2, Leica Microsystems) equipped with Metamorph v 2.1.39 (Olympus). Light microscopy images were grabbed with a Leica DC200 camera using Leica DC200 software (Leica). The software program ImageJ was used to fusion the images, and the image editing software Microsoft publisher was used to combine the obtained images into panels. The reference of the various brain structures was made according to the Franklin and Paxinos atlas "Mouse brain in stereotaxic coordinates" (39).

For the quantification of c-Fos immunoreactivity to light, the number of c-Fos-positive neurons in the SCN was counted by two independent experimenters blind to experimental conditions in an area of 300 × 500 μm at levels corresponding to bregma −0.30 to −0.70 mm (rostral to caudal part of the SCN) (Fig. 2 *A*, *viii*). Approximately nine brain sections from each animal containing the SCN (with AVP costaining) were analyzed, and c-Fos–positive cells were visually counted using a grid on each image. C-Fos immunoreactivity in response to light was analyzed using two-way ANOVA (light pulse and genotype conditions) followed by post hoc *t* tests.

Retinal Tract Tracing. After the completion of the recording protocol, SCNx and sham animals (sham *Opn4*$^{+/+}$ $n = 9$; sham *Opn4*$^{-/-}$ $n = 7$; SCNx *Opn4*$^{+/+}$ $n = 10$; SCNx *Opn4*$^{-/-}$ $n = 8$; WT $n = 7$; *Syt10*$^{Cre/Cre}$*Bmal1*$^{+/-}$ $n = 6$; and *Syt10*$^{Cre/Cre}$*Bmal1*$^{fl/-}$ $n = 8$) were anesthetized (isoflurane 2.5%, applied during all procedure), and 1 μl anterograde tracer CtB (1%, dissolved in 50 mM PBS, pH 7.4) was injected into the vitreous over 2 min. After 48 h, the animals were perfused, and the histology procedure was processed as described below.

Statistical Methodology. All statistics were calculated using standard methods with Statistica (Statsoft v. 8), and graphics were generated either in SigmaPlot (Systat v. 11) or Microsoft Excel (v. 2013). The differences in *n* values between certain light/dark regimes were due to ECoG/EMG signal problems on the day of recording. For ECoG spectrum analysis, some animals were excluded due to the increased number of signal artifacts, which allowed for the quantification of sleep and wake distribution, but hampered Fourier signal transformation. The differences in sleep amounts and quantitative ECoG variables were determined by single- or multiple-way ANOVAs followed by post hoc *t* tests if 5% significance levels were reached. The differences in the number of c-Fos–positive neurons were assessed by two-way (light and genotype conditions) ANOVA followed by post hoc *t* tests.

Data Availability. Data used to generate the anatomy figures in this manuscript are accessible on a public FigShare repository (DOI: 10.6084/m9.figshare.14176520). All other study data are included in the article and/or *SI Appendix*.

ACKNOWLEDGMENTS. We thank D. Ciocca and S. Reibel-Fosset, Chronobiotron-UMS3415, for their support with the mice colony and their advice on experiments and planning. This work was supported by grants from Alsace BioValley, France Région Grand-Est–Strasbourg Eurométropole, and Fondation Adiral. J.H. was supported by a fellowship from the French Ministry for Research and Higher Education and Fondation Adiral.

1. T. A. Bedrosian, R. J. Nelson, Influence of the modern light environment on mood. *Mol. Psychiatry* **18**, 751–757 (2013).
2. J. Falbe *et al.*, Sleep duration, restfulness, and screens in the sleep environment. *Pediatrics* **135**, e367–e375 (2015).
3. K. M. Stephenson, C. M. Schroder, G. Bertschy, P. Bourgin, Complex interaction of circadian and non-circadian effects of light on mood: Shedding new light on an old story. *Sleep Med. Rev.* **16**, 445–454 (2012).
4. G. Vandewalle, P. Maquet, D. J. Dijk, Light as a modulator of cognitive brain function. *Trends Cogn. Sci.* **13**, 429–438 (2009).
5. U. Kilic, J. Hubbard, P. Bourgin, "Circadian rhythm sleep disorders, 5. Treatment" in *Sleep Medicine Textbook*, C. Bassetti, Z. Dogas, P. Peigneux, Eds. (European Sleep Research Society, 2014), pp. 357–368.
6. A. A. Borbély, Effects of light on sleep and activity rhythms. *Prog. Neurobiol.* **10**, 1–31 (1978).
7. J. Hubbard, E. Ruppert, C. M. Gropp, P. Bourgin, Non-circadian direct effects of light on sleep and alertness: Lessons from transgenic mouse models. *Sleep Med. Rev.* **17**, 445–452 (2013).
8. C. Cajochen, Alerting effects of light. *Sleep Med. Rev.* **11**, 453–464 (2007).
9. N. Mrosovsky, Masking: History, definitions, and measurement. *Chronobiol. Int.* **16**, 415–429 (1999).
10. R. J. Lucas, M. S. Freedman, M. Muñoz, J. M. Garcia-Fernández, R. G. Foster, Regulation of the mammalian pineal by non-rod, non-cone, ocular photoreceptors. *Science* **284**, 505–507 (1999).
11. D. Lupi, H. Oster, S. Thompson, R. G. Foster, The acute light-induction of sleep is mediated by OPN4-based photoreception. *Nat. Neurosci.* **11**, 1068–1073 (2008).
12. J. W. Tsai *et al.*, Melanopsin as a sleep modulator: Circadian gating of the direct effects of light on sleep and altered sleep homeostasis in Opn4(-/-) mice. *PLoS Biol.* **7**, e1000125 (2009).
13. J. Hannibal, J. Fahrenkrug, Target areas innervated by PACAP-immunoreactive retinal ganglion cells. *Cell Tissue Res.* **316**, 99–113 (2004).
14. J. Hannibal *et al.*, Central projections of intrinsically photosensitive retinal ganglion cells in the macaque monkey. *J. Comp. Neurol.* **522**, 2231–2248 (2014).
15. S. Hattar *et al.*, Central projections of melanopsin-expressing retinal ganglion cells in the mouse. *J. Comp. Neurol.* **497**, 326–349 (2006).
16. S. Panda *et al.*, Melanopsin (Opn4) requirement for normal light-induced circadian phase shifting. *Science* **298**, 2213–2216 (2002).
17. N. F. Ruby *et al.*, Role of melanopsin in circadian responses to light. *Science* **298**, 2211–2213 (2002).
18. D. M. Berson, F. A. Dunn, M. Takao, Phototransduction by retinal ganglion cells that set the circadian clock. *Science* **295**, 1070–1073 (2002).
19. G. S. Lall *et al.*, Distinct contributions of rod, cone, and melanopsin photoreceptors to encoding irradiance. *Neuron* **66**, 417–428 (2010).
20. S. Hattar, H. W. Liao, M. Takao, D. M. Berson, K. W. Yau, Melanopsin-containing retinal ganglion cells: Architecture, projections, and intrinsic photosensitivity. *Science* **295**, 1065–1070 (2002).
21. I. Provencio, M. D. Rollag, A. M. Castrucci, Photoreceptive net in the mammalian retina. This mesh of cells may explain how some blind mice can still tell day from night. *Nature* **415**, 493 (2002).
22. A. D. Güler *et al.*, Melanopsin cells are the principal conduits for rod-cone input to non-image-forming vision. *Nature* **453**, 102–105 (2008).

23. H. C. van Diepen, A. Ramkisoensing, S. N. Peirson, R. G. Foster, J. H. Meijer, Irradiance encoding in the suprachiasmatic nuclei by rod and cone photoreceptors. *FASEB J.* **27**, 4204–4212 (2013).
24. C. M. Altimus *et al*., Rods-cones and melanopsin detect light and dark to modulate sleep independent of image formation. *Proc. Natl. Acad. Sci. U.S.A.* **105**, 19998–20003 (2008).
25. T. A. LeGates *et al*., Aberrant light directly impairs mood and learning through melanopsin-expressing neurons. *Nature* **491**, 594–598 (2012).
26. J. Husse, X. Zhou, A. Shostak, H. Oster, G. Eichele, Synaptotagmin10-Cre, a driver to disrupt clock genes in the SCN. *J. Biol. Rhythms* **26**, 379–389 (2011).
27. J. A. Evans *et al*., Shell neurons of the master circadian clock coordinate the phase of tissue clocks throughout the brain and body. *BMC Biol.* **13**, 43 (2015).
28. X. Jin *et al*., A molecular mechanism regulating rhythmic output from the suprachiasmatic circadian clock. *Cell* **96**, 57–68 (1999).
29. M. Mieda *et al*., Cellular clocks in AVP neurons of the SCN are critical for interneuronal coupling regulating circadian behavior rhythm. *Neuron* **85**, 1103–1116 (2015).
30. S. A. Rahman *et al*., Diurnal spectral sensitivity of the acute alerting effects of light. *Sleep (Basel)* **37**, 271–281 (2014).
31. G. Buzsáki, E. I. Moser, Memory, navigation and theta rhythm in the hippocampal-entorhinal system. *Nat. Neurosci.* **16**, 130–138 (2013).
32. C. S. Herrmann, M. H. Munk, A. K. Engel, Cognitive functions of gamma-band activity: Memory match and utilization. *Trends Cogn. Sci.* **8**, 347–355 (2004).
33. X. J. Wang, Neurophysiological and computational principles of cortical rhythms in cognition. *Physiol. Rev.* **90**, 1195–1268 (2010).
34. A. A. Borbély, A two process model of sleep regulation. *Hum. Neurobiol.* **1**, 195–204 (1982).
35. P. Franken, D. Chollet, M. Tafti, The homeostatic regulation of sleep need is under genetic control. *J. Neurosci.* **21**, 2610–2621 (2001).
36. P. Franken *et al*., NPAS2 as a transcriptional regulator of non-rapid eye movement sleep: Genotype and sex interactions. *Proc. Natl. Acad. Sci. U.S.A.* **103**, 7118–7123 (2006).
37. F. K. Stephan, I. Zucker, Circadian rhythms in drinking behavior and locomotor activity of rats are eliminated by hypothalamic lesions. *Proc. Natl. Acad. Sci. U.S.A.* **69**, 1583–1586 (1972).
38. T. I. Morgenthaler *et al*.; Standards of Practice Committee of the American Academy of Sleep Medicine, Practice parameters for the clinical evaluation and treatment of circadian rhythm sleep disorders. An American Academy of Sleep Medicine report. *Sleep* **30**, 1445–1459 (2007).
39. G. Paxinos, K. B. Franklin, *Paxinos and Franklin's the Mouse Brain in Stereotaxic Coordinates* (Academic Press, 2019).
40. J. Hubbard *et al*., Dataset for "Dissecting and modeling photic and melanopsin effects to predict sleep disturbances induced by irregular light exposure in mice." *FigShare*. http://dx.doi.org/10.6084/m9.figshare.14176520. Deposited 3 June 2021.